1 **Proteomic studies of the Arabidopsis TRAPP complexes reveal conserved**
2 **organization and a novel plant-specific component with a role in plant**
3 **development.**

4 Veder J. Garcia[1], Shou-Ling Xu[1], Raksha Ravikumar[2], Wenfei Wang[3], Liam Elliott[4],

5 Mary Fesenko[4], Melina Altmann[5], Pascal Falter-Braun[5,6], Ian Moore[4], Farhah F.

6 Assaad[2], Zhi-Yong Wang[1]*

7

8 *: corresponding author.

9

10 [1]Department of Plant Biology, Carnegie Institution for Science, Stanford, CA, 94305

11 [2]Plant Science Department, Botany, Technische Universität München, 85354 Freising,

12 Germany.

13 [3]Basic Forestry and Proteomics Research Center, Haixia Institute of Science and

14 Technology, Fujian Agriculture and Forestry University, Fuzhou, China

15 [4]Department of Plant Sciences, South Parks Road, Oxford, OX1 3RB, UK.

16 [5]Institute of Network Biology (INET), Helmholtz Zentrum München, Deutsches

17 Forschungszentrum für Gesundheit und Umwelt (GmbH), 85764 Neuherberg,

18 Germany.

19 [6]Faculty of Biology, Microbe-Host-Interactions, Ludwig-Maximilians-Universität (LMU)

20 München, 82152 Planegg-Martinsried, Germany.

21

22 *: corresponding author.

23 Department of Plant Biology

24 Carnegie Institution for Science

25 260 Panama St, Stanford, CA 94305, USA

26 EMAIL: zywang24@stanford.edu

27 TEL: 650-387-3800

28 FAX: 650-325-6857

29

30 **Running Title: TRAPP membrane trafficking complexes in plants**

31

Abstract

How the membrane trafficking system spatially organizes intracellular activities and intercellular signaling networks is not well understood in plants. The Transport Protein Particle (TRAPP) complexes are known to play key roles in selective delivery of membrane vesicles to various subcellular compartments in yeast and animals, but remain to be fully characterized in plants. Here we interrogate the TRAPP complexes in Arabidopsis using quantitative proteomic approaches. TRS33 is a component shared by all TRAPP complexes in yeast and animals, and the Arabidopsis AtTRS33 is essential for the subcellular dynamics of other TRAPP components. Affinity purification of AtTRS33 followed by quantitative mass spectrometry identified fourteen interacting proteins; these include not only thirteen homologs of all known TRAPP components in yeast and mammals but also a novel protein we named TRAPP-interacting plant protein (TRIPP), which is conserved in multi-cellular photosynthetic organisms. Proteomic and molecular analyses showed that TRIPP specifically associates with the TRAPPII complex *in vivo* and directly interacts with the TRAPPII-specific subunits but not the subunits shared with TRAPPIII. TRIPP co-localizes with a subset of TRS33 compartments, and its localization is disrupted in the *trs33* mutant. Loss-of-function *tripp* mutation caused growth and reproductive development defects, including partial photomorphogenesis in the dark. Our study demonstrates that plants possess at least two distinct TRAPP complexes similar to metazoan, and identifies TRIPP as a novel plant-specific component of the TRAPPII complex with important functions in plant growth and development.

Introduction

Vesicular protein trafficking is a highly organized and regulated cellular process that ensures delivery of proteins to their correct subcellular compartments (Rosquete and Drakakaki, 2018). Vesicle transport spatially organizes not only intracellular structures and metabolic activities, but also intercellular signaling systems that control development. Vesicle transport involves numerous protein complexes and is regulated at multiple stages, starting with vesicle budding from a donor membrane and ending

61   with the fusion stage, where a vesicle merges with a specific acceptor membrane

62   (Brocker et al., 2010). Prior to the fusion stage, tethering factors initiate and maintain

63   specific contact between donor and acceptor membranes to hold the vesicle in close

64   proximity to the target membrane (Whyte and Munro, 2002). Thus, tethering factors play

65   key role in organizing vesicle trafficking. However, the functions of tethering factors in

66   plant development remain largely uncharacterized.

67   In eukaryotes, there are two broad classes of tethering factors, long coiled-coil

68   proteins and multi-subunit tethering complexes (MTCs) (Brocker et al., 2010; Yu and

69   Hughson, 2010; Ravikumar et al., 2017; Takemoto et al., 2018). Coiled-coil tethers are

70   long, dimeric proteins that are found mainly on the Golgi and early endosomes (Lurick

71   et al., 2018), while MTCs contain several subunits in a modular form and are located on

72   organelles throughout the secretory and endocytic pathways. A well-studied MTC in

73   yeast and animals is the Transport Protein Particle (TRAPP) complex, which is involved

74   in Endoplasmic Reticulum (ER) to Golgi and Golgi-mediated trafficking as well as in

75   autophagy (Barrowman et al., 2010; Scrivens et al., 2011; Vukasinovic and Zarsky,

76   2016). In yeast, mutations in TRAPPs are typically lethal or cause strongly impaired

77   growth (Kim et al., 2016). In humans, mutations in TRAPP components have been

78   implicated in a variety of diseases (Milev et al., 2015; Sacher et al., 2018).

79   TRAPP complexes can exist in a variety of modular forms (Robinett et al., 2009;

80   Kim et al., 2016; Riedel et al., 2018). In yeast and metazoan, two TRAPP complexes (II

81   and III) composed of shared and complex-specific subunits have been confirmed

82   (Barrowman et al., 2010; Lynch-Day et al., 2010; Thomas et al., 2018). The metazoan

83   TRAPP complexes contain orthologues of all yeast TRAPP subunits, but have also

84   evolved additional subunits and rearrangement of complex composition. The TRAPPIII

85   complex contains two additional metazoan-specific subunits, TRAPPC11 and

86   TRAPPC12 (Scrivens et al., 2011; Zhao et al., 2017). Tca17 and Trs65 are TRAPPII-

87   specific subunits in yeast, but their metazoan orthologues (TRAPPC2L and TRAPPC13,

88   respectively) are found in TRAPPIII complexes. The subunit composition of TRAPP

89   complexes specifies localization and function. In yeast, TRAPPII functions in late Golgi

90   and TRAPPIII in early Golgi and autophagy (Kim et al., 2016; Riedel et al., 2018;

91   Thomas et al., 2018). In metazoans, TRAPPII is involved in membrane traffic in the
92   biosynthetic pathway, and TRAPPIII functions in autophagosome formation and
93   autophagy (Yamasaki et al., 2009; Scrivens et al., 2011; Bassik et al., 2013; Lamb et
94   al., 2016; Ramirez-Peinado et al., 2017; Sacher et al., 2018). Furthermore, TRAPP
95   complexes have been shown to function as Guanine nucleotide Exchange Factors
96   (GEF) for Rab GTPases in both yeast and metazoans (Jenkins et al., 2018; Riedel et
97   al., 2018; Thomas et al., 2018; Thomas et al., 2019).

98   In plants, TRAPP complex formation and modularity remain to be elucidated.
99   Although the Arabidopsis genome encodes orthologous TRAPP components, evidence
100   as to the existence of most TRAPP components at the protein level and whether or how
101   these assemble into TRAPP complexes is incomplete. Two Arabidopsis TRAPP
102   subunits have been characterized to some extent in plants; AtTRS120 and AtTRS130
103   (Jaber et al., 2010; Thellmann et al., 2010; Naramoto et al., 2014; Rybak et al., 2014).
104   Both AtTRS120/VAN4 and AtTRS130/CLUB are required for cell plate biogenesis.
105   Mutations in *AtTRS120* or *AtTRS130* cause seedling lethality and canonical
106   cytokinesis defective phenotypes, including cell wall stubs and incomplete cross walls
107   (Jaber et al., 2010; Thelmann et al., 2010; Qi et al., 2011). Also, in both mutants,
108   vesicles accumulate at the equator of dividing cells but fail to assemble into cell plates
109   (Jaber et al., 2010; Thellmann et al., 2010; Rybak et al., 2014; Ravikumar et al., 2017).
110   In accordance with TRAPP localization in other organisms, AtTRS120 and AtTRS130
111   localize at the *trans*-Golgi Network (TGN) (Qi et al., 2011; Naramoto et al., 2014;
112   Ravikumar et al., 2017; Ravikumar et al., 2018). Recently, in a genetic characterization,
113   the Arabidopsis orthologue of the yeast/metazoan shared subunit BET5 has been
114   shown to be essential for pollen exine pattern formation in Arabidopsis (Zhang et al.,
115   2018).

116   The above-mentioned studies provide strong evidence for critical functions of
117   TRAPP components in plants. Previous sequence analysis and proteomic studies have
118   predicted and identified partial TRAPP components, respectively (Drakakaki et al.,
119   2012; Paul et al., 2014; Rybak et al., 2014). However, experimental evidence is lacking
120   with regard to whether plants form the same number of TRAPP complexes as yeast and

4

121   metazoans, what the subunit composition of such complexes might be and whether

122   there are plant-specific TRAPP components. To address these questions, we have

123   taken a holistic proteomic approach to document the subunit composition and

124   interactors of TRAPP complexes in Arabidopsis. We identified eleven subunits that are

125   conserved in yeast and metazoans, and two that are only conserved between

126   metazoans and plants. Additionally, we identify and characterize a novel TRAPP

127   interacting plant protein (TRIPP) that is present only in multicellular photosynthetic

128   organisms. Genetic evidence shows that TRIPP plays an important role in plant growth,

129   reproduction, and light-dependent development. Our study demonstrates that

130   Arabidopsis TRAPP components form similar complexes as reported in metazoans. The

131   study also uncovers a novel plant-specific TRAPPII interactor that plays important roles

132   in plant growth and development.

RESULTS

AtTRS33 is required for the membrane association of a TRAPPII-specific subunit

135   Previous studies of TRAPP subunits in plants have partially revealed TRAPP

136   components, for instance, Drakakaki and her colleagues identified five TRAPP subunits

137   from isolated SYP61 TGN compartments in Arabidopsis using mass spectrometric

138   analysis (Drakakaki et al., 2012). A more recent AtTRS120 IP-MS study identified five

139   subunits, four overlapping with the results of Drakakaki et al. (Rybak et al., 2014).

140   However, a computational study that used OrthoMCL and PGAP algorithms to find

141   vesicular transport orthologues in yeast and plant genomes, identified at least nine

142   TRAPP components encoded in Arabidopsis (Paul et al., 2014).

143   To further identify protein components of TRAPP complexes in plants, we carried

144   out quantitative mass spectrometry analysis of proteins associated with TRS33, a

145   subunit known to be shared by different TRAPP complexes studied in both yeast and

146   metazoans (Kim et al., 2016; Riedel et al., 2018). We reasoned that an analysis of such

147   a shared subunit would give us a more comprehensive view of TRAPP complexes in

148   Arabidopsis than has thus far been available from studies based on TRAPPII-specific

149   subunits alone (Rybak et al., 2014; Ravikumar et al., 2018). In Arabidopsis, AtTRS33

5

150 has been implicated in cytokinesis and found in the TRAPPII interactome (Thellmann et
151 al., 2010; Rybak et al., 2014).

152   Prior to using TRS33 to further study TRAPP composition, we first sought to
153 confirm TRS33's functional relationship to TRAPPII in Arabidopsis. To this end, we
154 monitored the effect of *trs33-1* mutation on the localization dynamics of the TRAPPII-
155 specific subunit AtTRS120. In the wild type, the TRS120-GFP fusion protein localizes to
156 both the cytosol and to TGN compartments in interphase cells (Figure 1A; Rybak et al.,
157 2014; Ravikumar et al., 2018). In contrast, in the *trs33-1* mutant, the signal was only
158 observed in the cytosol, and no endomembrane compartments were detected (Figure
159 1A). This is reminiscent of the mis-localization of a TRAPPII-specific subunit (Trs130-
160 GFP) to the cytosol in *trs33* mutants of yeast (Tokarev et al., 2009). At early cytokinetic
161 stages, TRS120-GFP clearly localized to the cell plate in the wild type, but was present
162 as a diffuse cytosolic cloud around the cell plate in *trs33-1* (Figure 1B, 1D).
163 Furthermore, at the end of cytokinesis, TRS120-GFP re-localized to the leading edges
164 of the cell plate in the wild type but was, at best, visible as a weak and relatively diffuse
165 signal at the leading edges of *trs33-1* expanding cell plates (Figure 1C). Thus, AtTRS33
166 is required for the membrane association of AtTRS120 and for its proper localization
167 dynamics during cytokinesis. This establishes a clear functional link between AtTRS33
168 and the Arabidopsis TRAPPII complex.

169

170 **Quantitative mass spectrometry characterization of the TRAPP complexes**

171   To identify proteins associated with AtTRS33, we used <u>s</u>table <u>i</u>sotope <u>l</u>abeling
172 <u>i</u>mmuno<u>p</u>recipitation followed by quantitative <u>m</u>ass <u>s</u>pectrometry (SILIP-MS).
173 Transgenic Arabidopsis seedlings expressing AtTRS33 fused with Myc and His tags
174 from the native *AtTRS33* promoter (*TRS33:TRS33-MycHis*) in *trs33-1* mutant
175 background were grown for 14 days on medium containing light (^{14}N) nitrogen, along
176 with wild type as control grown on heavy (^{15}N) nitrogen. The isotopes were switched in
177 the replicate experiment. Root and shoot tissues were harvested separately. Each pair
178 of ^{14}N- and ^{15}N-labelled sample and control were mixed together before
179 immunoprecipitation with anti-Myc antibody beads (Figure 2A). Immunoprecipitated
180 proteins were separated by SDS-PAGE, in-gel digested and analyzed in an Orbitrap

181 mass spectrometer. Enrichment by TRS33 was quantified by the ^{14}N/^{15}N ratios of the

182 identified peptides. MS analysis identified over 1000 proteins in each experiment, but

183 only proteins that showed >2-fold enrichment in the TRS33-MycHis samples over the

184 controls in both forward and reciprocal labeling replicates were considered as TRS33

185 interactors. We identified fourteen TRS33-interacting proteins in samples from both

186 roots and shoots (Table I). SILIP-MS using transgenic Arabidopsis plants that

187 overexpress TRS33-YFP also identified the same 14 interacting proteins (Supplemental

188 Table I). These include all orthologues of the shared TRAPP subunits reported in yeast

189 and metazoans (TRS23, TRS33, TRS31, BET3, BET5, and TRS20) and of the

190 complex-specific subunits (TCA17, TRS120, TRS130, TRS85, TRAPPC11, TRAPC12,

191 and TRAPPC13) (Riedel et al., 2018; Sacher et al., 2018). Intriguingly, the identified

192 TRS33-associated proteins include an additional protein that has no orthologues in

193 yeast or metazoans (Figure 2B, Table I, Supplemental Table I, and Supplemental

194 Figure 1). This protein is composed of 838 amino acids and is listed as unknown in The

195 Arabidopsis Information Resource (TAIR) database. We named this protein TRAPP

196 Interacting Plant Protein (TRIPP). Taken together, the mass spectrometry results

197 demonstrate that plant TRAPP complexes contain not only homologs of all known

198 TRAPP components in yeast and metazoans, but also a plant-specific component

199 TRIPP.

200

201 **TRIPP behaves like a component of the TRAPP II complex in SILIP-MS**

202 **experiments.**

203   To confirm that TRIPP associates with TRAPP components and to determine

204 whether it is specific to a given TRAPP complex, we performed an additional SILIP-MS

205 using TRIPP as bait. Transgenic plants expressing TRIPP-YFP under a 35S promoter,

206 which complemented a *tripp-1* mutant, were grown along non-transgenic wild type as

207 control, as described above for TRS33 SILIP-MS experiment. The TRIPP-YFP and

208 associated proteins were Immunoprecipitated with anti-GFP antibody, and analyzed by

209 mass spectrometry (Figure 2A). The SILIP-MS data showed unambiguously that TRIPP

210 pulled down nine TRAPP subunits (Figure 3A, Supplemental Table II). These include all

211 six TRAPP shared subunits (TRS23, TRS33, TRS31, BET3, BET5, TRS20) and three

212　TRAPPII-specific subunits (TCA17, TRS120 and TRS130) (Figure 3A, 3B, 3C and
213　Supplemental Table II). Four TRAPP subunits (TRS85, TRAPPC11, TRAPPC12 and
214　TRAPPC13) identified in the TRS33 SILIP-MS showed no interaction with TRIPP in
215　these SILIP-MS experiments. None of these proteins were detected in both replicate
216　experiments or enriched by TRIPP-YFP in either single experiment. Interestingly, these
217　are homologs of the subunits specific to TRAPPIII in animals, suggesting that
218　Arabidopsis similarly possesses distinct TRAPPII and TRAPPIII complexes, and that
219　TRIPP specifically associates with the plant TRAPPII complex.

220

221　**TRIPP directly interacts with the TRAPPII-specific but not shared subunits.**

222　　　If TRIPP associates specifically with the TRAPPII complex, it likely interacts
223　directly with TRAPPII-specific subunits instead of the shared core subunits. To test this,
224　we performed yeast two-hybrid (Y2H) assays of binary TRIPP interactions with known
225　TRAPP subunits (Thellmann et al., 2010).　For the TRAPPII-specific subunits,
226　truncations were designed via phylogenetic analysis as described (Figure 3E, Steiner et
227　al., 2016b). In quadruplicate pairwise tests, TRIPP did not interact with shared TRAPP
228　subunits, including AtTRS33, but rather interacted specifically with the two TRAPPII-
229　specific subunits AtTRS120 and AtTRS130 (Figure 3D). Notably, strong interactions
230　were found with the plant-specific or poorly conserved domains of AtTRS130 (Figure
231　3D, 3E). Positive interactions were also observed with both extremities of AtTRS120
232　(Figure 3D). In conclusion, the plant-specific TRIPP protein interacts predominantly with
233　plant-specific domains of the large TRAPPII-specific subunits.

234

235　**TRIPP localizes to TGN/early endosomal compartments in Arabidopsis roots.**

236　　　Previous studies of TRAPPII specific subunits (e.g AtTRS120 and TRS130) show
237　localization to the *trans*-Golgi network/early endosome (TGN/EE) and to the cell plate
238　(Ravikumar et al., 2018). To examine TRIPP subcellular localization, we generated
239　transgenic plants expressing TRIPP-YFP under the 35S promoter in the *tripp-1* null
240　mutant background (mutant to be described later). Roots of transgenic seedlings
241　expressing TRIPP-YFP were analyzed by confocal imaging. TRIPP-YFP exhibited a
242　punctate localization signal that co-localized with FM4-64 (Figure 4A). TRIPP also

8

243 exhibited a cell plate localization similar to AtTRS120 and AtTRS130, both TRAPPII-
244 specific subunits (supplemental Figure 2A; Jaber et al., 2010; Rybak et al., 2014).
245 Further, co-localization at the cell plate was confirmed between TRIPP-YFP and
246 TRS120-mCherry in plants expressing both tagged proteins (Figure 4B). TRS33, a
247 subunit shared between different TRAPP complexes, exhibited a similar localization to
248 TRIPP (Supplemental Figure 2B). Co-localization of TRIPP and TRS33 was examined
249 by crossing *35S:TRIPP-mCherry* and *35S:TRS33-YFP* plants. In root cells from plants
250 co-expressing both proteins, all TRIPP-mCherry compartments are positive for TRS33-
251 YFP, whereas about 20% of the TRS33-YFP compartments show no TRIPP-mCherry
252 signal (Figure 4C). This is consistent with TRIPP being a component of only the
253 TRAPPII complex and TRS33 being in both TRAPPII and TRAPPIII complexes.
254 Furthermore, TRIPP-YFP localization is disrupted in the *trs33-1* mutant background
255 consistent with TRIPP being a TRAPP interacting component (Figure 4D). As TRAPPII
256 has been functionally linked to Rab-A GTPases in Arabidopsis (Qi et al., 2011; Qi and
257 Zheng 2011; Naramoto et al., 2014), we performed co-localization experiments with the
258 TGN/EE-localized RAB-A2a (Chow et al., 2008). This revealed that TRIPP co-localized
259 with YFP-RAB-A2a (Figure 4E). To confirm TRIPP localization to TGN is not due to
260 TRAPPII potential interaction with RABs, we perform co-localization with another
261 TGN/EE resident Vesicle transport v-SNARE 12 (VTI12) (Geldner et. al., 2009).
262 Consistently, we observed TRIPP co-localization with VTI12 (Supplemental Figure 2C).
263 Taken together, the data provides *in vivo* evidence that TRIPP co-localizes with
264 TGN/EE-markers and associated TRAPPII subunits (Qi et al., 2011; Naramoto et al.,
265 2014; Ravikumar et al., 2018).

266

267 **The Arabidopsis *tripp* mutant displays growth defects including partial**
268 **photomorphogenesis in the dark.**

269 To explore TRIPP's role in plant development, we performed phenotypic
270 characterization of *tripp-1*, an insertion allele where a T-DNA is inserted in the 5th exon
271 of the *TRIPP* gene, which has 10 exons and renders a null mutation (Figure 5A,
272 Supplemental Figure 3A, 3B). The *tripp-1* homozygous plants exhibited smaller rosettes
273 compared to wild type (WT) and were sterile (Figure 5B, 5C). Plants heterozygous for

274 the T-DNA insertion did not exhibit a phenotype, and thus the *tripp-1* mutation was

275 maintained in heterozygous plants. To confirm that the phenotypes observed were due

276 to the specific mutation in the *TRIPP* gene, a transgene containing the 35S promoter

277 driving a full-length TRIPP coding sequence fused to YFP was introduced by

278 Agrobacterium transformation to the TRIPP +/- heterozygous plants. Plants expressing

279 TRIPP-YFP in the *tripp-1* homozygous background fully rescued the phenotypes

280 observed in the *tripp-1* mutant (Figure 5), confirming that the observed phenotypes were

281 due to loss of function of TRIPP. Both mutant and WT bolted at similar times but

282 inflorescences were prominently shorter in the mutant (Figure 5C). Floral organs

283 appeared normal in the mutant, with the exception that anthers failed to produce pollen,

284 thus no seeds were produced (Fig 5D). The anthers of the *tripp-1* mutant had a smooth

285 surface suggesting pollen development defects occur in early stages of anther

286 development. To determine whether the *tripp-1* mutant has any defects in the female

287 gametophyte, WT pollen was used to pollinate *tripp-1* mutant flowers. Although the

288 mutant stigma appeared normal, flowers pollinated with WT pollen did not produce any

289 seeds, suggesting that *tripp-1* has defects in both male and female reproductive

290 development. Overall, the *tripp-1* mutant exhibits similar sterility but weaker dwarfism

291 phenotypes compared to the *trs33-1* mutant (Figure 5E-5G). Taken together, our

292 genetic analyses indicate that TRIPP has important functions throughout plant growth

293 and development and particularly for reproductive development.

294   The dwarf phenotype of light-grown *tripp-1* mutant led us to compare *tripp-1*

295 growth and cell elongation in the dark versus light (skotomorphogenesis vs

296 photomorphogenesis). When seeds were placed on medium in the light, seeds

297 germinated at the same time, hypocotyl length was similar between *tripp-1* and WT, but

298 *tripp-1* mutant had shorter roots (Figure 6A-6C). Conversely, in the dark, although the

299 *tripp-1* mutant and WT germinated at the same time, the *tripp-1* mutant exhibited a

300 shorter hypocotyl but longer root compared to WT (Figure 6D-6F). Furthermore, the

301 *tripp-1* mutant grown in the dark for two-weeks developed true leaves, while the WT did

302 not (Supplemental Figure 4). To determine if cell elongation and anisotropy are

303 disrupted in *tripp-1*, the hypocotyl cells of dark-grown and light-grown seedlings were

304 visualized with propidium iodide staining. In the dark, *tripp-1* exhibited prominently

shorter cells than WT, whereas light-grown *tripp-1* seedlings showed similar cell size as WT (Figure 6G and 6H). These observations indicate that TRIPP plays an important role in photomorphogenesis.

TRIPP is present in the green lineage with the exception of chlorophytes

Sequence analysis indicate TRIPP is present in streptophytes (multicellular algae to flowering plants) (Supplemental Figure 5A). TRIPP homologues are found as far as the charophycean algae, which are multicellular photosynthetic organisms ancestral to land plants, but surprisingly not present in unicellular photosynthetic chlorophytes such as chlamydomonas. This is in contrast to other TRAPP components such as the shared TRAPP subunit TRS33, which is present from chlorophytes to embryophytes and across kingdoms (Supplemental Figure 5B; Kim et al., 2016). Protein alignment of TRIPP protein sequence indicates high conservation among its homologues (Supplemental Figure 5C). These analyses indicate that TRIPP might have evolved early in the streptophytes, parallel to the emergence of multicellularity in plants.

Discussion

The endomembrane system is crucial for cellular organization and morphogenesis, and is regulated by complex networks of proteins and protein-complexes in eukaryotes. The TRAPP complexes have been extensively characterized in yeast and metazoans, and have been shown genetically to play important roles in the endomembrane system in plants, yet the protein components of the TRAPP complex and their functions in plant development remain to be characterized in plants. Our quantitative IP-MS experiments demonstrate that in Arabidopsis TRAPP complexes contain homologues of all thirteen mammalian TRAPP subunits. In addition, the TRAPPII complex associates with an additional plant specific component, which plays important roles in a range of developmental processes including photomorphogenesis.

The Arabidopsis TRAnsport Protein Particle (TRAPP) complexes include fourteen subunits

11

335   Proteomic approaches provide a valuable tool for the characterization of protein-
336   protein interactions and protein complexes in various organisms (Takac et al., 2017).
337   Surprisingly, all previous proteomic studies combined have only identified six TRAPP
338   components in Arabidopsis, in contrast to 11 and 13 subunits in yeast and animals,
339   respectively (Drakakaki et al., 2012; Rybak et al., 2014). For instance, in metazoans,
340   the TRAPPII complex is composed of seven 'shared' subunits and three TRAPPII-
341   specific subunits (Figure 6; Scrivens et al., 2011; Riedel et al., 2018; Sacher et al.,
342   2018). While TRAPPIII contains the same shared subunits as TRAPPII, plus four
343   TRAPPIII-specific subunits, including two metazoan-specific not found in yeast (Figure
344   7; Scrivens et al., 2011; Zhao et al., 2017). Based on our understanding of TRAPP
345   structure in yeast and animals, we focused on using an essential shared subunit
346   combined with quantitative mass spectrometry to identify TRAPP-interacting proteins.
347   TRS33 is a shared TRAPP subunit in yeast and animals, and in Arabidopsis our initial
348   data indicated that AtTRS33 is required for the membrane association of TRS120 (a
349   component of TRAPPII) and for its localization dynamics during cytokinesis (Figure 1).
350   Combined with our earlier findings that *trs33-1* mutants are, like *trappii* mutants,
351   impaired in cytokinesis (Thellmann et al., 2010), this established a function of AtTRS33
352   as a key component of the TRAPP complexes.

353   In contrast to previous studies (Drakakaki et al., 2012; Rybak et al., 2014), our
354   quantitative IP-MS analysis of AtTRS33 identified fourteen TRAPP interacting proteins,
355   which include homologs of all the TRAPP components known in yeast and animals, as
356   well as a plant-specific protein, TRIPP. We carried out multiple SILIP-MS experiments,
357   each including two replicates, with shoot and root tissues of transgenic plants
358   expressing TRS33 from either the native *TRS33* promoter or the 35S promoter, as well
359   as with different affinity tags. Although more than 1000 proteins were detected by mass
360   spectrometry, accurate quantitation enabled by stable isotope labelling identified only
361   the TRAPP subunit homologs and TRIPP as TRS33-associated proteins. No other
362   proteins showed over 2-fold enrichment by TRS33 in both replicate experiments, and no
363   RAB was found enriched in even a single experiment. It is likely that our stringent
364   washing condition prevented detection of dynamic interactors. But this supports, on the
365   other hand, that TRIPP is a relatively stable component of the TRAPP complex. As

12

366   such, our high-quality SILIP-MS data identified a more complete set of TRAPP complex

367   components, some of which have not been previously reported to be present in plants.

368   These proteins include homologs of all yeast and metazoan TRAPP subunits, and

369   TRIPP as a new component that has homologs in multicellular photosynthetic

370   organisms but not in fungi or metazoans.

371

372   **TRIPP is a plant-specific TRAPPII-associated component**

373   Among studies of TRAPP proteins in different organisms, it is known that animals

374   possess two additional TRAPP subunits (TRAPPC11 and TRAPPC12) compared to

375   yeast (Kim et al., 2016; Riedel et al., 2018). This suggests that multicellular organisms

376   might have evolved a more complex regulation of, or novel functions for, TRAPP

377   components. The human TRAPPC12, for example, has been implicated in kinetochore

378   assembly and mitosis through association with chromosomes (Milev et al., 2015).

379   Interestingly, among the fourteen Arabidopsis TRAPP interactors, TRIPP was found to

380   be specific to plants and is currently classified as an unknown protein in plant

381   databases. Protein sequence analysis and database mining indicate that, based on

382   protein homology, TRIPP is specific to multicellular photosynthetic organisms

383   (Supplemental Figure 6A). This is in contrast to other TRAPP subunits such as TRS33,

384   which is present in all eukaryotes including unicellular algae and flowering plants

385   (Supplemental Figure 5B).

386   Our biochemical and genetic data strongly support that TRIPP is specifically

387   associated with TRAPPII, a complex that has been shown to be involved in post-Golgi

388   membrane trafficking (Ravikumar et al., 2018). While the SILIP-MS analysis of AtTRS33

389   interactome identified fourteen subunits, the TRIPP SILIP-MS identified only ten

390   subunits that include the specific subunits of TRAPPII but exclude those of TRAPPIII.

391   The presence of the homologs of the four animal TRAPPIII-specific subunits

392   (TRAPPC8, TRAPPC11, TRAPPC12, and TRAPPC13) in the AtTRS33 interactome but

393   not the TRIPP interactome suggests the existence of both TRIPP-containing TRAPPII

394   complex and an equivalent of TRAPPIII complex that excludes TRIPP. Indeed, in

395   accordance with our results, a recent IP-MS using AtTRAPPC11 has confirmed the

396   presence of a TRAPPIII complex in Arabidopsis (Rosquette et al., 2019). Our Y2H data

13

397   indicates that TRIPP interacts with the two TRAPPII-specific subunits TRS120 and
398   TRS130, further corroborating TRIPP association with the TRAPPII complex. Consistent
399   with these molecular interactions, TRIPP co-localizes with AtTRS33 at some endosomal
400   compartments presumably in the TRAPPII complex, but is absent at a subset of
401   AtTRS33-containing endosomal compartments, which are likely TRAPPIII-specific
402   (Figure 4C). These results support that TRIPP is a specific component of TRAPPII.

403   The TRAPPII complex is well conserved in yeast and animals, with the exception
404   of the TRS65 subunit, which in yeast associates with TRAPPII and in animals with
405   TRAPPIII (Choi et al., 2011). Now we show that TRAPPII is also conserved in plants
406   but, as in animal models, TRS65 does not associate with TRAPPII. Thus, plant TRAPP
407   complexes seem more similar to metazoan than to yeast complexes. Our results
408   demonstrate that multi-cellular plants have evolved TRIPP as a plant-specific
409   component of the TRAPPII complex, whereas TRAPPIII is conserved in animals and
410   plants (Figure 7).

411   TRAPPII is known to associate with the TGN, which is a hub for membrane
412   trafficking; exocytosis, endocytosis and protein sorting (Qi et al., 2011; Naramoto et al.,
413   2014; Ravikumar et al., 2018). Arabidopsis TRAPPII subunits, TRS120 and TRS130,
414   localize to endosomes, the *trans*-Golgi network, and cell plates during cytokinesis
415   (Ravikumar et al., 2017; Ravikumar et al., 2018). Our study shows that TRIPP exhibits a
416   similar localization to TGN/EE compartments as well as cell plate. The disruption of
417   TRIPP localization in the *trs33* mutant supports that TRIPP localization to membrane
418   compartments is dependent on the TRAPP complexes.

419

420   **TRIPP plays critical roles in plant growth, reproduction and light-dependent**
421   **development**

422   The *tripp-1* mutant exhibits a range of developmental phenotypes, including
423   partial dwarfism, shorter roots, and sterility in light-grown plants. The sterility phenotype
424   is similar to that observed in the *trs33-1* mutant (Supplemental Figure 4). Mutations of
425   the TRAPPII specific components in plants cause detrimental phenotypes (Thellmann et
426   al., 2010; Rybak et al., 2014; Ravikumar et al., 2017). The overall growth phenotypes of
427   *tripp-1* are weaker than the *trs33*, or *trs120* and *trs130* mutants, which have lethal

14

phenotypes past the early seedling stage. These observations suggest that TRIPP association with TRAPPII provides specific functions, in contrast to the broader functions of AtTRS120 and AtTRS130. As TRIPP is only present in multicellular photosynthetic organisms, while other TRAPPII components are present in all eukaryotes including algae, it is conceivable that TRIPP may play important roles in development and/or environmental adaptation in multicellular plants. Indeed, the phenotypes of *tripp* mutants grown in the dark suggest a role in photomorphogenesis (Figure 6). While membrane trafficking is critical for proper cell growth, and any defect in vesicle traffic regulation can cause hypocotyl growth defects (He et al., 2018), the dark-grown *tripp-1* mutant seedlings exhibit not only shorter hypocotyls but also longer roots, a hallmark of photomorphogenesis. These results demonstrate that TRIPP, and likely the TRAPPII complex, plays a role in light-regulated plant development. Our proteomic and genetic study provides a framework for future studies of TRAPP complex functions in cellular membrane trafficking and plant development.

METHODS

Plant materials

Arabidopsis thaliana ecotype Columbia (Col-0) was used in this study. Plants were grown in greenhouses with a 16-h light/ 8-h dark cycle at 22°C for general growth and seed harvesting. For seedling analysis such as dark germination or for root imaging, plants were grown on petri dishes as follows: seeds were surface-sterilized with 70% ethanol+0.1%Triton X-100 for 5 mins, dried on a filter paper and then grown on ½ Murashige and Skoog (MS) medium, 1% sucrose and 0.8% phytoagar. Plates with seeds were stratified at 4 $^{\circ}$C for 3 days and then placed in a growth chamber under 16hr light/8hr dark (or complete dark for germination in the dark) at 22°C.

T-DNA insertional mutant, *tripp-1* (SALKseq_063596.3) was obtained from the Arabidopsis Biological Resource Center (www.arabidopsis.org; Alonso et al., 2003). *trs33-1* (SALK_109244) is from our previously published work (Thellmann et al., 2010).

Construction of plasmid and generation of transgenic plants

15

458   Full-length coding sequences for AtTRS33 and TRIPP without stop codons were
459 cloned into *pENTR/SD/D-TOPO* (Invitrogen). To generate *35S-TRS33-YFP* and *35S-*
460 *TRIPP-YFP* constructs, each entry clone was sub-cloned into Gateway-compatible
461 destination vector *pEarleyGate-101* using LR clonase (Invitrogen). To generate *35S-*
462 *TRIPP-mCherry*, entry clone was subcloned into *pEarleyGate 101* vector that carries
463 the mCherry tag instead of YFP. For native promoter driven TRS33-4XMyc-6XHis, an
464 entry clone was generated using a 1kb genomic region upstream of TRS33 start site
465 fused with TRS33 full coding sequence and sub-cloned into a gateway compatible
466 *pCAMBIA1390* vector. For co-localization with YFP-RabA2a, TRIPP was cloned from
467 Arabidopsis (Columbia) genomic DNA into *pUB-RFP-DEST-HygR* (derived from Grefen
468 et al., 2010). Constructs were validated by nucleotide sequencing. All binary vector
469 constructs were introduced into Agrobacterium tumefaciens (strain GV3101) and
470 transgenic plants generated Arabidopsis by floral dipping (Clough and Bent, 1998).
471 *TRS120:TRS120-GFP* and *PUBQ:TRS120-mCherry* are described in Rybak et al.,
472 2014 and *YFP-Rab-A2a* in Chow et al., 2008.

473

474 **[15]N Stable-isotope-labeling in Arabidopsis quantitative MS analysis of the**
475 **AtTRS33 interactome.**
476 The pTRS33:TRS33-MycHis and wild-type plants were grown for two weeks at 22°C
477 with 24 hours light on vertical ^{14}N or ^{15}N medium plates (½ Murashige & Skoog modified
478 basal salt mixture without nitrogen 0.39g/L, 8g/L phytoblend, and 1g/L KNO_3 or 1g/L
479 $K^{15}NO_3$ (Cambridge Isotope Laboratories) for ^{14}N medium or ^{15}N medium, respectively,
480 pH5.8). About 2.5 g of tissue was harvested for each sample, ^{14}N-labeled TRS33-Myc-
481 His and ^{15}N-labeled wild type samples or reciprocal (^{14}N-labeled wild type and [15]N-
482 labeled TRS33-Myc-His) were mixed, then ground in liquid nitrogen and stored in -
483 80°C. Immunoprecipitation was performed as followed; proteins were extracted in 10
484 mL NEBT buffer (20 mM HEPES, pH7.5, 40 mM KCl, 1 mM EDTA, 10% glycerol, 0.5%
485 Triton X-100, 1 mM phenylmethylsulfonyl fluoride (PMSF), Pierce protease inhibitor
486 cocktail (Thermo Fisher), and PhosStop cocktail (Roche)), centrifuged at 5,000rpm for 5
487 min, supernatant (SP) transferred to new tube and centrifuged a second time for 15 min
488 at 14,000 rpm, then SP transferred to new tube. The SP was incubated with 10µl of

16

489 Myc-Trap®_MA (chromotek) and incubated for 1 hour. Next, beads were washed 3X

490 with 1ml immunoprecipitation buffer without detergent. Proteins were eluted with 2X

491 SDS buffer. The eluted proteins were separated by SDS-PAGE. After Coomassie

492 Brillant blue staining, the protein bands were excited and subjected to in-gel digestion

493 with trypsin.

494 The peptide mixtures were desalted using C18 ZipTips (Millipore) and analyzed

495 on a Q-Exactive HF hybrid quadrupole-Orbitrap mass spectrometer (Thermo Fisher)

496 equipped with an Easy LC 1200 UPLC liquid chromatography system (Thermo Fisher).

497 Peptides were separated using analytical column ES803 (Thermo Fisher). The flow rate

498 was 300nL/min and a 120-min gradient was used. Peptides were eluted by a gradient

499 from 3 to 28% solvent B (80% acetonitrile/0.1 formic acid) over 100 mins and from 28 to

500 44% solvent B over 20 mins, followed by short wash at 90% solvent B. Precursor scan

501 was from mass-to-charge ratio (m/z) 375 to 1600 and top 20 most intense multiply

502 charged precursor were selection for fragmentation. Peptides were fragmented with

503 higher-energy collision dissociation (HCD) with normalized collision energy (NCE) 27.

504 Tandem mass spectrometry peak lists were extracted using an in-house script PAVA,

505 and data were searched using Protein Prospector (Chalkley et al., 2008) against the

506 *Arabidopsis* Information Resource (TAIR10) database, to which reverse sequence

507 versions were concatenated (a total of 35,386 entries) to allow estimation of a false

508 discovery rate (FDR). Carbamidomethylcysteine was searched as a fixed modification

509 and oxidation of methionine, Peptide N-terminal Gln conversion to pyroglutamate and

510 N-terminal acetylation as variable modifications. Data were searched with a 10 ppm

511 tolerance for precursor ion and 20 ppm for fragment ions. Peptide and protein FDRs

512 were set as 0.01 and 0.05. ^{15}N labeled amino acids were also searched as a fixed

513 modification for ^{15}N data. Quantification was done using Protein Prospector.

514 Note that for the IP-MS of p35S-TRS33-YFP vs wild-type or p35S-TRIPP-YFP vs wild-

515 type the same method described above was used with the difference that GFP-trap

516 magnetic agarose beads (Allele) were used instead for immunoprecipitation.

517

518

519 **Yeast Two-Hybrid (Y2H)**

520   Y2H screens were performed as described (Dreze et al., 2010). TRAPPII-specific

521   (AtTRS120 and CLUB/AtTRS130) truncations are described in Steiner et al., 2016;

522   shared TRAPP subunits were obtained from Riken full length cDNA clones(Seki et al.,

523   2002) or from a collection of 12,000 Arabidopsis ORFs(Wessling et al., 2014). We used

524   the GAL4 DNA-binding domain (DB) encoded in Y2H vector pDEST-pPC97,

525   subsequently transformed into the yeast strain Y8930, as well as gene fusions to the

526   Gal4 activation domain (AD) in the yeast strain Y8800 (Altmann et al., 2018). Both

527   strains are derived from PJ68-4 (James et al., 1996). The constructs were screened by

528   yeast mating in quadruplicate pair-wise tests. Screening was done as a binary mini-pool

529   screen, i.e. each DB-ORF was screened against pools of 188 AD-ORFs. Interactions

530   were assayed by growth on selective plates using the HIS3 reporter, and using 1mM 3-

531   Amino-1,2,4-triazole (3-AT) to suppress background growth. This primary screen was

532   carried out once and interaction candidates were identified by Sanger sequencing. All

533   candidate interactions were verified by pairwise one-on-one mating in three

534   independent experiments. Only pairs scoring positives in all three assays were

535   considered as bona fide interaction partners.

536

537

538   **Confocal microscopy**.

539   Plant roots were imaged on an Olympus (www.olympus-ims.com) Fluoview 1000

540   confocal laser scanning microscope (CSLM), a Leica TCS SP8 microscope (www.leica-

541   microsystems.com) and a Zeiss 880 CLSM (www.zeiss.com/microscopy). Imaging data

542   were acquired using LAS-X software (Leica) and professed on Fiji/image J software

543   (www.imagej.com). The following excitation and emission parameters were used for the

544   respective fluorescent proteins: YFP 514nm excitation, 525-575nm emission; GFP

545   488nm excitation, 500-550nm emission; mCherry 561nm excitation, 580-643nm

546   emission; mRFP 561nm excitation, 581-754nm emission; and FM4-64 emission at 700-

547   725 nm. For Figure 1, cell cycle stages were determined via TRS120-GFP localization

548   dynamics, taking into account how this membrane marker follows phragmoplast

549   microtubule dynamics (Steiner et al., 2016a). As *trapp* mutants affect both cell plate

550   biogenesis and phragmoplast microtubule dynamics (Steiner et al., 2016a), we also

551   relied on FM4-64 to image cell plates in *trapp* mutants. Based on the appearance of the

552   cell plate, cytokinesis was broadly split into early stages (cell plate initiation and

553   biogenesis) versus late stages (cell plate insertion and maturation; (Smertenko et al.,

554   2017). For quantification of co-localization analysis, image background was subtracted

555   from both channels; in the resultant background-subtracted images, co-localization

556   between intracellular YFP: RAB-A2a and TRIPP: mRFP1 was quantified using

557   Pearson's Correlation Coefficient using the JACoP Fiji plugin (Costes et al., 2004; Bolte

558   and Cordelieres, 2006).

559

560   **Accession numbers**

561   Sequence data from this article can be found in the GenBanK/EMBL data libraries

562   under the following accession numbers: TRS33, AT3G05000; TRIPP, AT3G17900;

563   BET5, AT1G51160; TRS20, AT1G80500; TCA17, AT2G20930; BET3, AT5G54750;

564   TRS23, AT5G02280; TRS31, AT5G58030; TRS85, AT5G16280; TRS120, AT5G11040

565   ;TRS130, AT5G54440;TRAPPC11, AT5G65950;TRAPPC12, AT4G39820;TRAPPC13,

566   AT2G47960; RAB-A2a, At1g09630.

567

568   All data that support the conclusions of this study are available from the corresponding

569   author upon request.

570

571   **Supplemental Information**

572   Supplemental Table 1. 35S-TRS33-YFP SILIP-MS results from roots and shoots.

573   Supplemental Table 2. 35S-TRIPP-YFP SILIP-MS results with additional information

574   such as peptide number and fold change.

575   Figure S1. Mass Spectrum of a TRIPP peptide identified in TRS33-MycHis SILIP-MS.

576   Figure S2. TRIPP cell plate localization and TRS33 localization and additional TGN

577   marker colocalization.

578   Figure S3. *tripp-1* T-DNA genotyping and mRNA analysis by RT-PCR

579   Figure S4. Two-week dark grown *tripp-1.*

580   Figure S5. TRIPP phylogenetic and protein alignment.

581

582

AUTHOR CONTRIBUTIONS:

V.J.G. performed all experiments, with the exception of those mentioned below, and wrote the manuscript.

Z.W. conceived the research project, designed experiments, and edited the manuscript.

S.X. and W.W. performed mass spectrometry analyses.

R.R. generated, analyzed and assembled data shown in Figure 1 under the supervision of F.F.A.

L.E., M.F., and I.M. provided constructs and performed the experiment shown in Fig. 4E.

L.E. edited the manuscript.

M.A. and R.R. performed yeast-two-hybrid experiments in Figure 3 under the supervision of F.F.A and P. F-B.

F.F.A. designed experiments, performed crosses, analyzed data, drafted sections of and edited the manuscript.

Z.W., F.F.A., S.X., and P.F-B. acquired funding.

20

619

620

621   REFERENCES

622   Alonso, J.M., Stepanova, A.N., Leisse, T.J., Kim, C.J., Chen, H., Shinn, P., Stevenson,
623   D.K., Zimmerman, J., Barajas, P., Cheuk, R., Gadrinab, C., Heller, C., Jeske, A.,
624   Koesema, E., Meyers, C.C., Parker, H., Prednis, L., Ansari, Y., Choy, N., Deen,
625   H., Geralt, M., Hazari, N., Hom, E., Karnes, M., Mulholland, C., Ndubaku, R.,
626   Schmidt, I., Guzman, P., Aguilar-Henonin, L., Schmid, M., Weigel, D., Carter,
627   D.E., Marchand, T., Risseeuw, E., Brogden, D., Zeko, A., Crosby, W.L., Berry,
628   C.C., and Ecker, J.R. (2003). Genome-wide insertional mutagenesis of
629   Arabidopsis thaliana. Science (New York, N.Y.) 301, 653-657.
630   Altmann, M., Altmann, S., Falter, C., and Falter-Braun, P. (2018). High-Quality Yeast-2-
631   Hybrid Interaction Network Mapping. Current protocols in plant biology 3,
632   e20067.
633   Barrowman, J., Bhandari, D., Reinisch, K., and Ferro-Novick, S. (2010). TRAPP
634   complexes in membrane traffic: convergence through a common Rab. Nat Rev
635   Mol Cell Biol 11, 759-763.
636   Bassik, M.C., Kampmann, M., Lebbink, R.J., Wang, S., Hein, M.Y., Poser, I.,
637   Weibezahn, J., Horlbeck, M.A., Chen, S., Mann, M., Hyman, A.A., Leproust,
638   E.M., McManus, M.T., and Weissman, J.S. (2013). A systematic mammalian
639   genetic interaction map reveals pathways underlying ricin susceptibility. Cell 152,
640   909-922.
641   Bolte, S., and Cordelieres, F.P. (2006). A guided tour into subcellular colocalization
642   analysis in light microscopy. Journal of microscopy 224, 213-232.
643   Brocker, C., Engelbrecht-Vandre, S., and Ungermann, C. (2010). Multisubunit tethering
644   complexes and their role in membrane fusion. Curr Biol 20, R943-952.
645   Chalkley, R.J., Baker, P.R., Medzihradszky, K.F., Lynn, A.J., and Burlingame, A.L.
646   (2008). In-depth analysis of tandem mass spectrometry data from disparate
647   instrument types. Molecular & cellular proteomics : MCP 7, 2386-2398.
648   Choi, C., Davey, M., Schluter, C., Pandher, P., Fang, Y., Foster, L.J., and Conibear, E.
649   (2011). Organization and assembly of the TRAPPII complex. Traffic 12, 715-725.
650   Chow, C.M., Neto, H., Foucart, C., and Moore, I. (2008). Rab-A2 and Rab-A3 GTPases
651   define a trans-golgi endosomal membrane domain in Arabidopsis that contributes
652   substantially to the cell plate. Plant Cell 20, 101-123.

653 Costes, S.V., Daelemans, D., Cho, E.H., Dobbin, Z., Pavlakis, G., and Lockett, S.
654 (2004). Automatic and quantitative measurement of protein-protein colocalization
655 in live cells. Biophysical journal 86, 3993-4003.
656 Drakakaki, G., van de Ven, W., Pan, S., Miao, Y., Wang, J., Keinath, N.F., Weatherly,
657 B., Jiang, L., Schumacher, K., Hicks, G., and Raikhel, N. (2012). Isolation and
658 proteomic analysis of the SYP61 compartment reveal its role in exocytic
659 trafficking in Arabidopsis. Cell Res 22, 413-424.
660 Dreze, M., Monachello, D., Lurin, C., Cusick, M.E., Hill, D.E., Vidal, M., and Braun, P.
661 (2010). Chapter 12 - High-Quality Binary Interactome Mapping. B.-M. in
662 Enzymology ed. (Academic Press), pp. 281–315.
663 Geldner, N., Dénervaud-Tendon, V., Hyman, D. L., Mayer, U., Stierhof, Y. D., & Chory,
664 J. (2009). Rapid, combinatorial analysis of membrane compartments in intact
665 plants with a multicolor marker set. The Plant Journal, 59(1), 169-178.
666 Grefen, C., Donald, N., Hashimoto, K., Kudla, J., Schumacher, K., and Blatt, M.R.
667 (2010). A ubiquitin-10 promoter-based vector set for fluorescent protein tagging
668 facilitates temporal stability and native protein distribution in transient and stable
669 expression studies. Plant J 64, 355-365.
670 Jaber, E., Thiele, K., Kindzierski, V., Loderer, C., Rybak, K., Jurgens, G., Mayer, U.,
671 Sollner, R., Wanner, G., and Assaad, F.F. (2010). A putative TRAPPII tethering
672 factor is required for cell plate assembly during cytokinesis in Arabidopsis. New
673 Phytol 187, 751-763.
674 James, P., Halladay, J., and Craig, E.A. (1996). Genomic libraries and a host strain
675 designed for highly efficient two-hybrid selection in yeast. Genetics 144, 1425-
676 1436.
677 Jenkins, M.L., Margaria, J.P., Stariha, J.T.B., Hoffmann, R.M., McPhail, J.A., Hamelin,
678 D.J., Boulanger, M.J., Hirsch, E., and Burke, J.E. (2018). Structural determinants
679 of Rab11 activation by the guanine nucleotide exchange factor SH3BP5. Nat
680 Commun 9, 3772.
681 Kim, J.J., Lipatova, Z., and Segev, N. (2016). TRAPP Complexes in Secretion and
682 Autophagy. Front Cell Dev Biol 4, 20.
683 Lamb, C.A., Nuhlen, S., Judith, D., Frith, D., Snijders, A.P., Behrends, C., and Tooze,
684 S.A. (2016). TBC1D14 regulates autophagy via the TRAPP complex and ATG9
685 traffic. EMBO J 35, 281-301.
686 Lurick, A., Kummel, D., and Ungermann, C. (2018). Multisubunit tethers in membrane
687 fusion. Curr Biol 28, R417-R420.
688 Lynch-Day, M.A., Bhandari, D., Menon, S., Huang, J., Cai, H., Bartholomew, C.R.,
689 Brumell, J.H., Ferro-Novick, S., and Klionsky, D.J. (2010). Trs85 directs a Ypt1
690 GEF, TRAPPIII, to the phagophore to promote autophagy. Proc Natl Acad Sci U
691 S A 107, 7811-7816.
692 Milev, M.P., Hasaj, B., Saint-Dic, D., Snounou, S., Zhao, Q., and Sacher, M. (2015).
693 TRAMM/TrappC12 plays a role in chromosome congression, kinetochore
694 stability, and CENP-E recruitment. J Cell Biol 209, 221-234.
695 Naramoto, S., Nodzylski, T., Dainobu, T., Takatsuka, H., Okada, T., Friml, J., and
696 Fukuda, H. (2014). VAN4 encodes a putative TRS120 that is required for normal
697 cell growth and vein development in Arabidopsis. Plant Cell Physiol 55, 750-763.

Paul, P., Simm, S., Mirus, O., Scharf, K.D., Fragkostefanakis, S., and Schleiff, E. (2014). The complexity of vesicle transport factors in plants examined by orthology search. PLoS One 9, e97745.

Qi, X., Kaneda, M., Chen, J., Geitmann, A., and Zheng, H. (2011). A specific role for Arabidopsis TRAPPII in post-Golgi trafficking that is crucial for cytokinesis and cell polarity. Plant J 68, 234-248.

Ramirez-Peinado, S., Ignashkova, T.I., van Raam, B.J., Baumann, J., Sennott, E.L., Gendarme, M., Lindemann, R.K., Starnbach, M.N., and Reiling, J.H. (2017). TRAPPC13 modulates autophagy and the response to Golgi stress. J Cell Sci 130, 2251-2265.

Ravikumar, R., Steiner, A., and Assaad, F.F. (2017). Multisubunit tethering complexes in higher plants. Curr Opin Plant Biol 40, 97-105.

Ravikumar, R., Kalbfuss, N., Gendre, D., Steiner, A., Altmann, M., Altmann, S., Rybak, K., Edelmann, H., Stephan, F., Lampe, M., Facher, E., Wanner, G., Falter-Braun, P., Bhalerao, R.P., and Assaad, F.F. (2018). Independent yet overlapping pathways ensure the robustness and responsiveness of trans-Golgi network functions in Arabidopsis. Development 145.

Riedel, F., Galindo, A., Muschalik, N., and Munro, S. (2018). The two TRAPP complexes of metazoans have distinct roles and act on different Rab GTPases. J Cell Biol 217, 601-617.

Robinett, C.C., Giansanti, M.G., Gatti, M., and Fuller, M.T. (2009). TRAPPII is required for cleavage furrow ingression and localization of Rab11 in dividing male meiotic cells of Drosophila. J Cell Sci 122, 4526-4534.

Rosquete, M. R., Worden, N., Ren, G., Sinclair, R. M., Pfleger, S., Salemi, M., ... & Drakakaki, G. (2019). AtTRAPPC11/ROG2: A Role for TRAPPs in Maintenance of the Plant trans-Golgi Network/Early Endosome Organization and Function. The Plant Cell, tpc-00110.

Rosquete, M.R., and Drakakaki, G. (2018). Plant TGN in the stress response: a compartmentalized overview. Curr Opin Plant Biol 46, 122-129.

Rosquete, M.R., Davis, D.J., and Drakakaki, G. (2018). The Plant Trans-Golgi Network: Not Just a Matter of Distinction. Plant Physiol 176, 187-198.

Rybak, K., Steiner, A., Synek, L., Klaeger, S., Kulich, I., Facher, E., Wanner, G., Kuster, B., Zarsky, V., Persson, S., and Assaad, F.F. (2014). Plant cytokinesis is orchestrated by the sequential action of the TRAPPII and exocyst tethering complexes. Dev Cell 29, 607-620.

Sacher, M., Shahrzad, N., Kamel, H., and Milev, M.P. (2018). TRAPPopathies: An emerging set of disorders linked to variations in the genes encoding transport protein particle (TRAPP)-associated proteins. Traffic.

Scrivens, P.J., Noueihed, B., Shahrzad, N., Hul, S., Brunet, S., and Sacher, M. (2011). C4orf41 and TTC-15 are mammalian TRAPP components with a role at an early stage in ER-to-Golgi trafficking. Molecular biology of the cell 22(12), 2083-2093.

Seki, M., Narusaka, M., Kamiya, A., Ishida, J., Satou, M., Sakurai, T., Nakajima, M., Enju, A., Akiyama, K., Oono, Y., Muramatsu, M., Hayashizaki, Y., Kawai, J., Carninci, P., Itoh, M., Ishii, Y., Arakawa, T., Shibata, K., Shinagawa, A., and Shinozaki, K. (2002). Functional annotation of a full-length Arabidopsis cDNA collection. Science (New York, N.Y.) 296, 141-145.

744 Smertenko, A., Assaad, F., Baluska, F., Bezanilla, M., Buschmann, H., Drakakaki, G.,
745   Hauser, M.T., Janson, M., Mineyuki, Y., Moore, I., Muller, S., Murata, T., Otegui,
746   M.S., Panteris, E., Rasmussen, C., Schmit, A.C., Samaj, J., Samuels, L.,
747   Staehelin, L.A., Van Damme, D., Wasteneys, G., and Zarsky, V. (2017). Plant
748   Cytokinesis: Terminology for Structures and Processes. Trends in cell biology 27,
749   885-894.
750 Steiner, A., Muller, L., Rybak, K., Vodermaier, V., Facher, E., Thellmann, M.,
751   Ravikumar, R., Wanner, G., Hauser, M.T., and Assaad, F.F. (2016a). The
752   Membrane-Associated Sec1/Munc18 KEULE is Required for Phragmoplast
753   Microtubule Reorganization During Cytokinesis in Arabidopsis. Molecular plant 9,
754   528-540.
755 Steiner, A., Rybak, K., Altmann, M., McFarlane, H.E., Klaeger, S., Nguyen, N., Facher,
756   E., Ivakov, A., Wanner, G., Kuster, B., Persson, S., Braun, P., Hauser, M.T., and
757   Assaad, F.F. (2016b). Cell cycle-regulated PLEIADE/AtMAP65-3 links membrane
758   and microtubule dynamics during plant cytokinesis. Plant J 88, 531-541.
759 Takac, T., Samajova, O., and Samaj, J. (2017). Integrating cell biology and proteomic
760   approaches in plants. J Proteomics 169, 165-175.
761 Takemoto, K., Ebine, K., Askani, J.C., Kruger, F., Gonzalez, Z.A., Ito, E., Goh, T.,
762   Schumacher, K., Nakano, A., and Ueda, T. (2018). Distinct sets of tethering
763   complexes, SNARE complexes, and Rab GTPases mediate membrane fusion at
764   the vacuole in Arabidopsis. Proc Natl Acad Sci U S A 115, E2457-E2466.
765 Thellmann, M., Rybak, K., Thiele, K., Wanner, G., and Assaad, F.F. (2010). Tethering
766   factors required for cytokinesis in Arabidopsis. Plant Physiol 154, 720-732.
767 Thomas, L.L., Joiner, A.M.N., and Fromme, J.C. (2018). The TRAPPIII complex
768   activates the GTPase Ypt1 (Rab1) in the secretory pathway. J Cell Biol 217, 283-
769   298.
770 Thomas, L.L., van der Vegt, S.A., and Fromme, J.C. (2019). A steric Gating Mechanism
771   Dictates the Substrate Speficity of a Rab-GEF. Developmental Cell 48, 1-15.
772 Tokarev, A.A., Taussig, D., Sundaram, G., Lipatova, Z., Liang, Y., Mulholland, J.W., and
773   Segev, N. (2009). TRAPP II complex assembly requires Trs33 or Trs65. Traffic
774   10, 1831-1844.
775 Vukasinovic, N., and Zarsky, V. (2016). Tethering Complexes in the Arabidopsis
776   Endomembrane System. Front Cell Dev Biol 4, 46.
777 Wessling, R., Epple, P., Altmann, S., He, Y., Yang, L., Henz, S.R., McDonald, N., Wiley,
778   K., Bader, K.C., Glasser, C., Mukhtar, M.S., Haigis, S., Ghamsari, L., Stephens,
779   A.E., Ecker, J.R., Vidal, M., Jones, J.D., Mayer, K.F., Ver Loren van Themaat, E.,
780   Weigel, D., Schulze-Lefert, P., Dangl, J.L., Panstruga, R., and Braun, P. (2014).
781   Convergent targeting of a common host protein-network by pathogen effectors
782   from three kingdoms of life. Cell Host Microbe 16, 364-375.
783 Whyte, J.R., and Munro, S. (2002). Vesicle tethering complexes in membrane traffic. J.
784   Cell Sci 115, 2627-2637.
785 Yamasaki, A., Menon, S., Yu, S., Barrowman, J., Meerloo, T., Oorschot, V.,
786   Klumperman, J., Satoh, A., and Ferro-Novick, S. (2009). mTrs130 is a
787   component of a mammalian TRAPPII complex, a Rab1 GEF that binds to COPI-
788   coated vesicles. Molecular biology of the cell 20(19), 4205-4215.

24

789 Yip, C.K., Berscheminski, J., and Walz, T. (2010). Molecular architecture of the
790   TRAPPII complex and implications for vesicle tethering. Nat Struct Mol Biol 17,
791   1298-1304.
792 Yu, I.M., and Hughson, F.M. (2010). Tethering factors as organizers of intracellular
793   vesicular traffic. Annu Rev Cell Dev Biol 26, 137-156.
794 Zhang, J., Chen, J., Wang, L., Zhao, S., Li, J., Liu, B., Li, H., Qi, X., Zheng, H., and Lu,
795   M. (2018). AtBET5 is essential for exine pattern formation and apical meristem
796   organization in Arabidopsis. Plant Sci 274, 231-241.
797 Zhao, S., Li, C.M., Luo, X.M., Siu, G.K., Gan, W.J., Zhang, L., Wu, W.K., Chan, H.C.,
798   and Yu, S. (2017). Mammalian TRAPPIII Complex positively modulates the
799   recruitment of Sec13/31 onto COPII vesicles. Sci Rep 7, 43207.

800
801
802
803
804
805
806
807
808
809
810
811
812
813
814
815
816
817
818
819
820
821
822
823

824

825

826

827

TRAPP subunits identified by TRS33 Immunoprecipitation from *Arabidopsis* roots									
	Forward			Reciprocal					
Gene ID	Peptide No.	% Cov	L/H ratio	Peptide No.	% Cov	L/H ratio	Protein Name	Yeast Orthologue	Human Orthologue
AT1G51160	5	41.4	4.47	4	28.4	0.41	BET5	BET5	TRAPPC1
AT1G80500	3	28.9	4.13	3	28.9	0.29	TRS20	TRS20	TRAPPC2
AT2G20930	6	52.9	3.79	5	52.9	0.39	TCA17	TCA17	TRAPPC2L
AT5G54750	12	55.4	11.4	12	54.3	0.18	BET3[a,b]	BET3	TRAPPC3
AT5G02280	5	42.6	2.72	-	-	-	TRS23	TRS23	TRAPPC4
AT5G58030	5	22.6	2.48	2	10.3	0.37	TRS31[a,b]	TRS31	TRAPPC5
AT3G05000	11	61.3	7.7	11	60.7	0.07	TRS33[a,b]	TRS33	TRAPPC6
AT5G16280	16	11.7	7.27	13	9.5	0.15	TRS85[a]	TRS85	TRAPPC8
AT5G11040	32	32.7	3.62	23	25.6	0.40	TRS120/VAN4[a,b]	TRS120	TRAPPC9
AT5G54440	33	31	4.19	13	12.3	0.44	TRS130/CLUB[b]	TRS130	TRAPP10
AT5G65950	20	17.6	7.76	12	11.2	0.18	TRAPPC11	-	TRAPPC11
AT4G39820	15	35.8	8.06	8	21.3	0.24	TRAPPC12	-	TRAPPC12
AT2G47960	14	37.1	2.84	14	33.3	0.52	TRS65	TRS65	TRAPPC13
AT3G17900	22	30.4	3.54	19	24.8	0.39	TRIPP	-	-
TRAPP subunits identified by TRS33 Immunoprecipitation from *Arabidopsis* shoots									
	Forward			Reciprocal					
Gene ID	Peptide No.	% Cov	L/H ratio	Peptide No.	% Cov	L/H ratio	Protein Name	Yeast orthologue	Human Orthologue
AT1G51160	4	34.9	14.7	2	14.2	0.16	BET5	BET5	TRAPPC1
AT1G80500	1	8.9	12.9	2	20	0.10	TRS20	TRS20	TRAPPC2
AT2G20930	6	63.6	3.9	4	36.4	0.36	TCA17	TCA17	TRAPPC2L
AT5G54750	12	55.4	30.2	11	46.8	0.07	BET3[a,b]	BET3	TRAPPC3
AT5G02280	6	51.8	7.1	-	-	-	TRS23	TRS23	TRAPPC4
AT5G58030	4	29.2	11.9	6	29.7	0.14	TRS31[a,b]	TRS31	TRAPPC5
AT3G05000	12	74.0	37.9	8	52.6	0.04	TRS33[a,b]	TRS33	TRAPPC6
AT5G16280	16	12.7	10.3	13	8.6	0.12	TRS85[a]	TRS85	TRAPPC8
AT5G11040	24	22.5	5.5	19	18.6	0.23	TRS120/VAN4[a,b]	TRS120	TRAPPC9
AT5G54440	23	20.2	4.7	18	17.1	0.27	TRS130/CLUB[b]	TRS130	TRAPP10
AT5G65950	27	22.8	12.8	13	12.4	0.12	TRAPPC11	-	TRAPPC11
AT4G39820	9	24.3	15.3	10	24.3	0.11	TRAPPC12	-	TRAPPC12
AT2G47960	14	32.4	5.2	12	30.5	0.26	TRS65	TRS65	TRAPPC13
AT3G17900	19	28.6	3.8	17	21.1	0.32	TRIPP	-	-

828 **Table I. Fourteen Arabidopsis TRAPP components were identified by stable isotope labeling**

829 **immunoprecipitation mass spectrometry (SILIP-MS).** SILIP-MS was performed using the

830 *TRS33*:*TRS33-4MycHis*/*trs33-1* complemented plants (Root and Shoot separately). Number of unique

831 peptides (Peptide No.), percentage of sequence coverage (% Cov), and ratio of signal intensities between

832 samples labelled with light (L, ^{14}N) and heavy (H, ^{15}N) isotopes (L/H ratio) are shown for two biological

26

833   replicates, in which either the Col-0 control (Forward) or the TRS33-MycHis sample (Reciprocal) was

834   labelled with [15]N. [a]Subunits previously identified in a proteomic study using isolated TGN compartments

835   (Drakaki et. al, 2012). [b]Subunits previously identified in label-free IP-MS of AtTRS130 (Rybak et al 2014).

836   Yeast and human orthologue names are based on published work (Thomas et al., 2018 and Riedel et al,

837   2018, respectively).
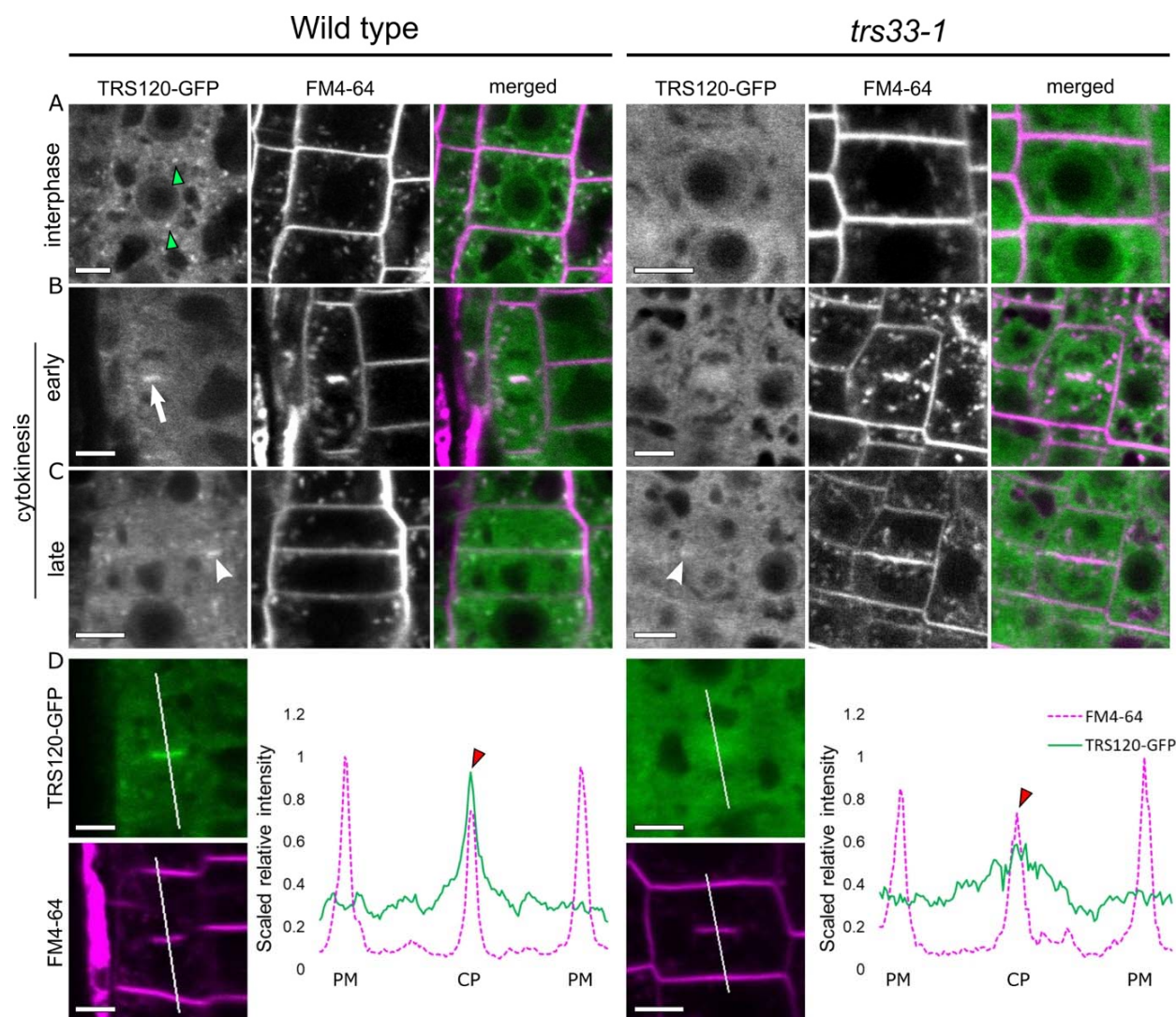
838

839

840

841

842

843

844

845

846

Figure 1. TRS33 is required for normal subcellular localization of TRS120-GFP.
Live imaging of TRS120-GFP (green) and FM4-64 (magenta in the merged panels) in roots of *TRS120:TRS120-GFP* plants. CP cell plate. PM: plasma membrane.
A. Cells at interphase show TRS120-GFP enriched at endomembrane compartments in the wild type (green arrowheads) but not in *trs33-1*, where only a cytosolic haze can be seen.
B. At early cytokinetic stages (CP initiation and biogenesis), TRS120-GFP is enriched at the cell plate (white arrow) in the wild type but not in *trs33-1*
C. At late cytokinetic stages (CP insertion and maturation), TRS120-GFP reorganizes to the leading edges of the cell plate (white arrowhead) in the wild type. In contrast, only a weak and relatively diffuse TRS120-GFP signal can be detected at the leading edges of the cell plate in *trs33-1* mutants (white arrowhead).
D. Line graphs depicting scaled relative fluorescence intensities. A sharp peak is seen at the CP in the wild type (red arrowhead) but not in *trs33-1*.
At least ten seedlings were imaged per marker line. n = 8 wild type, n = 7 *trs33-1* cytokinetic cells. Size bars = 5µm.
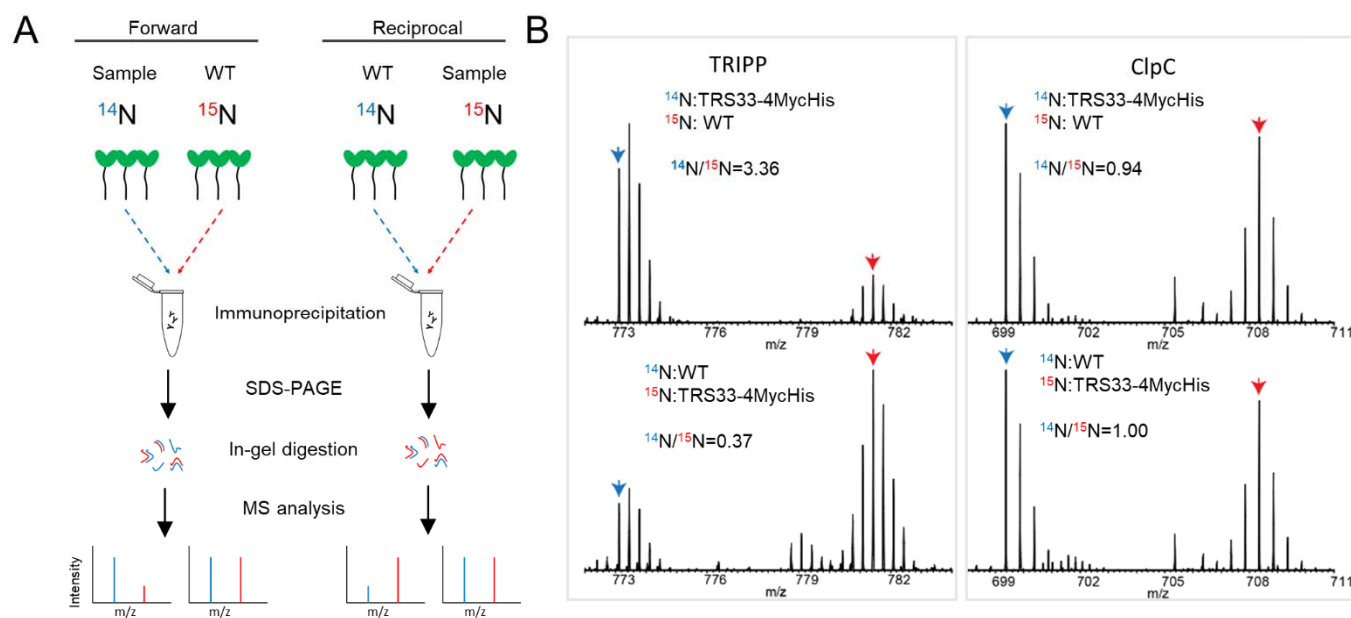
Figure 2. TRAPP-associated proteins were identified by Immunoprecipitation of TRS33

A. Experimental work flow for the Stable Isotope Labeling Immunoprecipitation Mass Spectrometry (SILIP-MS) in Arabidopsis.

B. MS1 spectra show the enrichment of TRIPP in SILIP-MS of TRS33:TRS33-4MycHis/*trs33-1* versus Wild type (Col-0) control, and no enrichment of ClpC, a non-specific protein. Blue and red rows point to monoisotopic peaks of [14]N- and ^{15}N-labeled peptides, respectively.
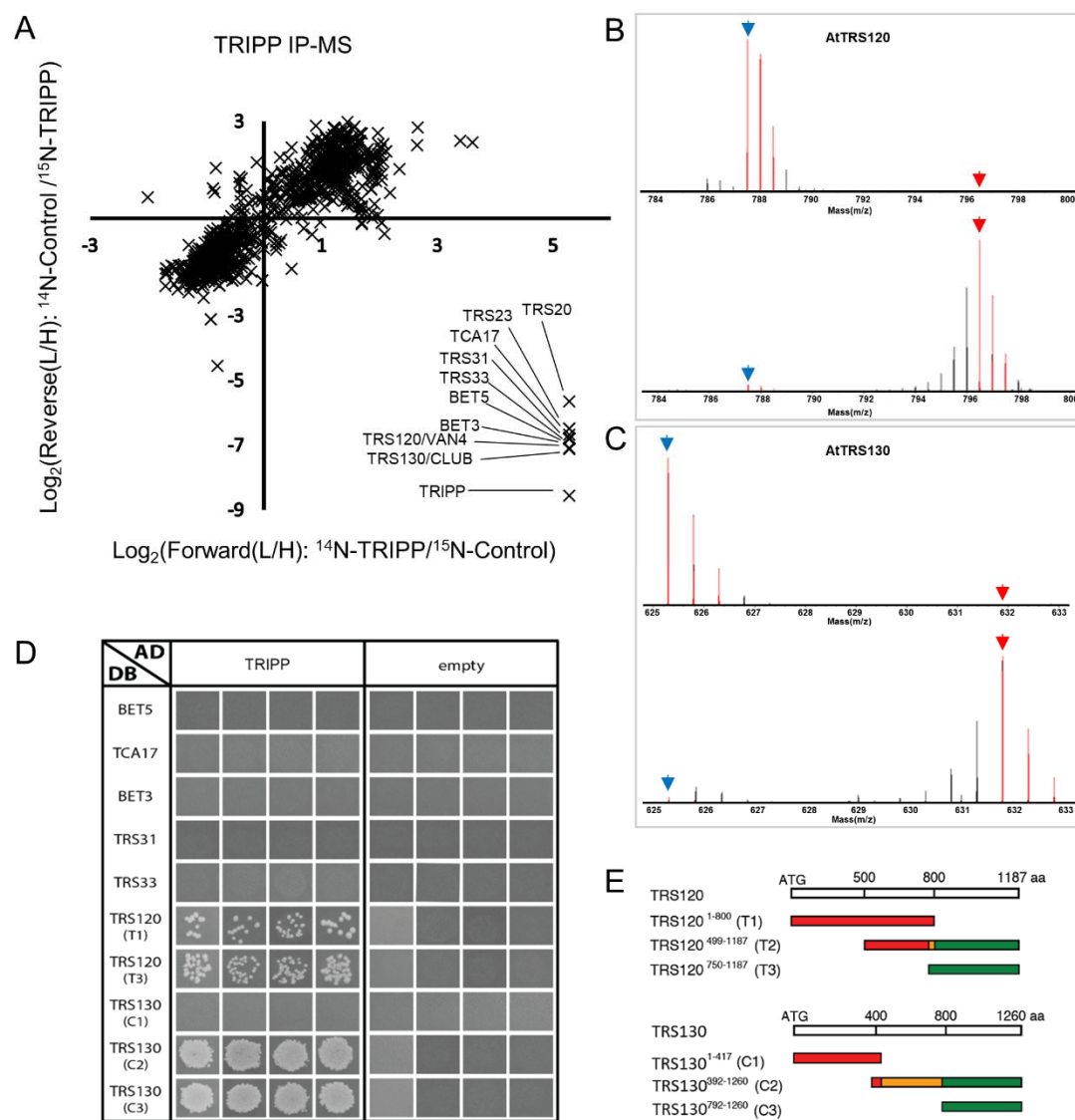
872

Figure 3. TRIPP interacts with TRAPPII subunits.

A. Metabolic stable isotope labeling immunoprecipitation mass spectrometry (SILIP-MS) analysis of TRIPP identifies only TRAPPII subunits. SILIP-MS was performed using *35S:TRIPP-YFP/tripp-1* complemented plants. Plot shows $\log_2$ ratio of signal intensities between samples labelled with light (L, ^{14}N) and heavy (H, ^{15}N) isotopes (L/H ratio) for two biological replicates, in which either the Col-0 control (Forward) or the TRIPP-YFP sample (Reciprocal) was labelled with ^{15}N. Note that TRAPP-III subunits are not identified in the data set.

B. Representative spectra of an AtTRS120 peptide quantified in the SILIP-MS experiments of ^{14}N-TRIPP-YFP vs ^{15}N-Col-0 (upper panel) and ^{14}N-Col-0 vs ^{15}N-TRIP-YFP (lower panel). Blue and red arrow points to mono-isotopic peak of the ^{14}N and ^{15}N labeled peptide respectively.

C. Representative spectra of an AtTRS130 peptide quantified in the TRIPP-YFP SILIP-MS experiments as descried for panel B.

D. Yeast two-hybrid assays of interactions between TRIPP and TRAPP subunits. The panels are from different plates. Four independent replicate experiments were performed. The results show interactions of TRIPP with both T1 and T3 regions of AtTRS120 and with the plant specific C2/C3_DB AtTRS130 regions. T2_DB is not included as it is an auto activator, as evidenced by colony growth with the empty AD vector, and this precludes our ability to determine whether AtTRS120_T2 interacts with TRIPP.

30

890   **E.** TRAPPII coding regions used for yeast two-hybrid interaction assays. Segments colored in red are
891   conserved across kingdoms, while those in green are plant-specific. The orange moiety of the C2
892   segment is poorly conserved across kingdoms. The T2 middle segment corresponds to sequences found
893   to interact with the exocyst in a yeast two-hybrid screen (Rybak et al., 2014).
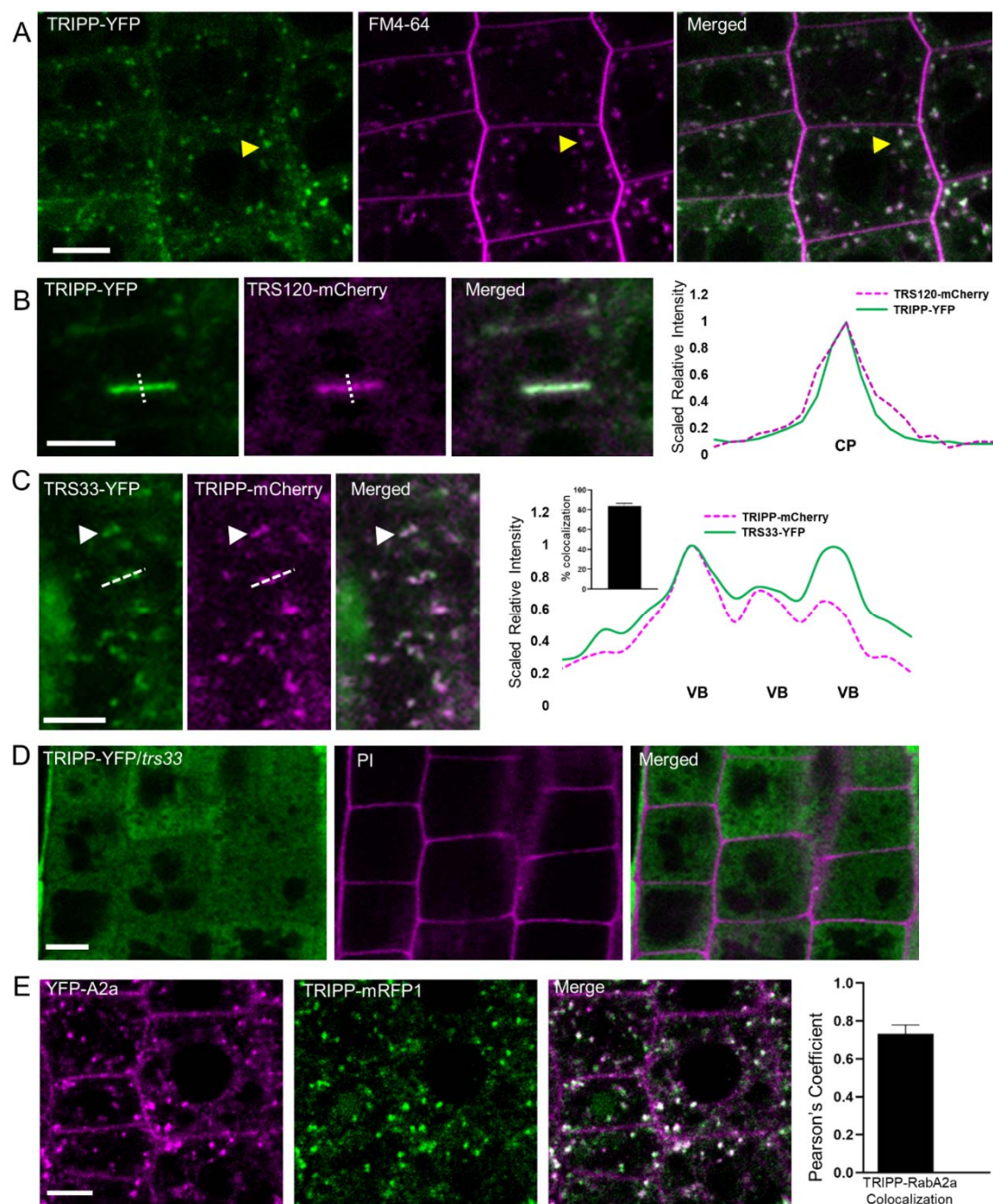
894

895

Figure 4. TRIPP localizes to vesicles and the cell plate, similar to known TRAPP components, and its localization disrupted in *trs33-1* mutant background.

A) Confocal images show TRIPP-YFP and FM4-64 staining signals in the roots of the *35S:TRIPP-YFP*/*tripp* complemented transgenic plants. Arrowhead indicates co-localization of TRIPP-YFP with FM4-64 positive TGN/endocytic vesicles.

B) TRIPP-YFP co-localizes with TRS120-mCherry to cell plates. Dashed line show the position of the intensity plot. CP = cell plate.

C) Roots of plants transformed with both *35S:TRS33-YFP* and *35S:TRIPP-mCherry* show co-localization (white arrow head) of TRIPP to some but not all vesicles in which TRS33-YFP localizes to. Dashed lines

905   in the image show the position of the quantification graph on the right panel. VB: vesicle bodies, Inset
906   graph shows percent colocalization of TRIPP-mCherry to TRS33-YFP-containing compartments. n = 7.
907   **D)** TRIPP-YFP localization is disrupted in the *trs33-1* mutant background. Root cell walls stained with
908   propidium iodide.
909   **E)** *UBQ10:TRIPP-mRFP1* transgenic plants show TRIPP-mRFP1 colocalization with the TGN marker
910   YFP-RabA2a (Chow et al., 2008). Graph shows co-localization quantification analyzed by Pearson's
911   correlation coefficient. n = 20 cells.
912   Scale bar for all panels = 5 µm
913
914
915
916
917
918
919
920
921
922
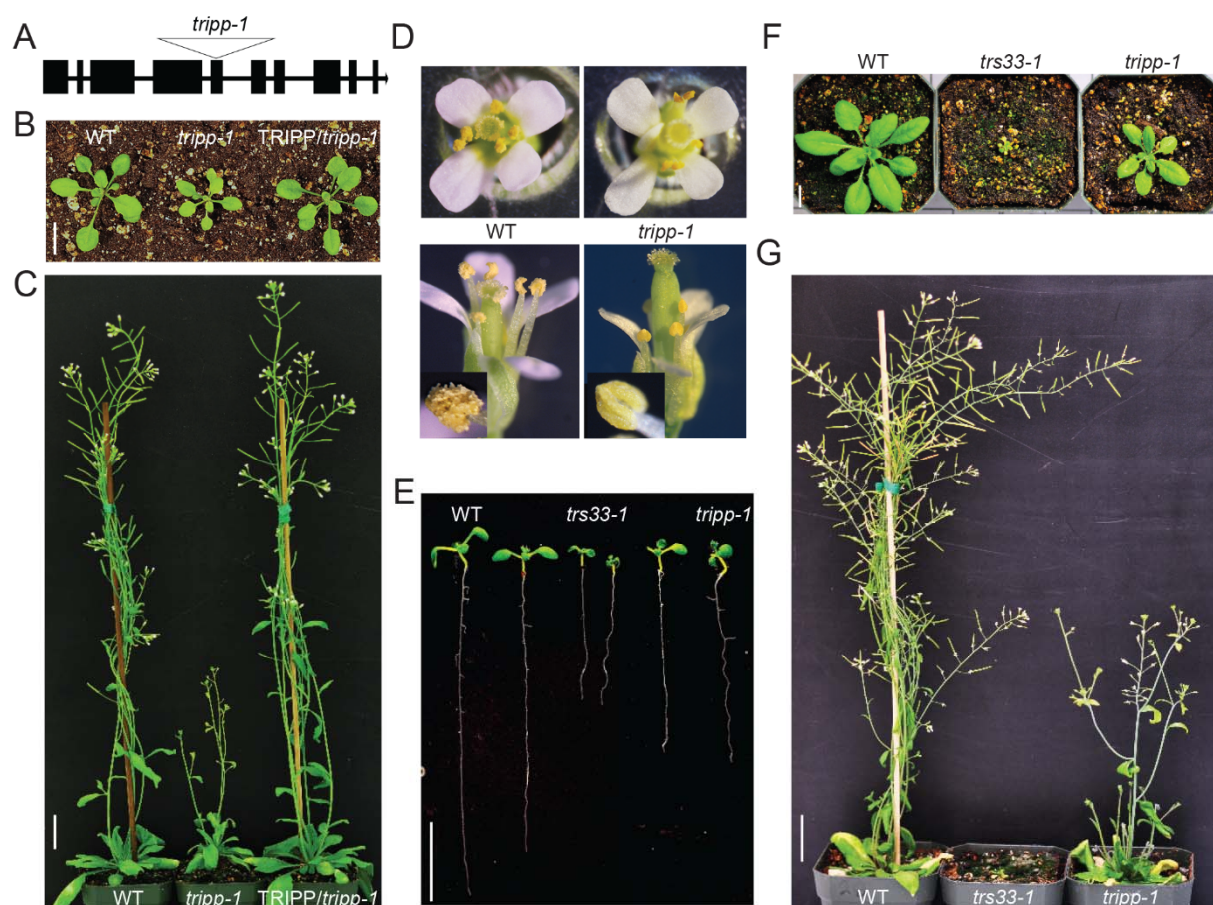923
924
925
926
927
928
929
930

33

Figure 5. The *tripp* mutant exhibits dwarfism and sterility

A. Gene model of Arabidopsis *TRIPP*/AT3G17900 gene shows the T-DNA insertion (Salkseq_063596) of *tripp-1* located in the fifth exon.

B. Two-week old *tripp-1* mutant plants grown in 16hr light / 8hr dark cycles show smaller rosette compared to WT and the *35S:TRIPP-YFP*/*tripp-1* plants (*TRIPP-YFP*/*tripp-1)*. Scale bar = 1 cm.

C. Five-week old *tripp-1* mutant plants grown in 16hr light / 8hr dark cycle exhibit significantly shorter inflorescence compare to WT and the *TRIPP-YFP/tripp*-1 plants. Scale bar = 1 inch.

D. Flowers of *tripp-1* plants appear normal, but anthers lack pollen. Insets of lower panel show magnified images of anthers.

E. and **F.** The *tripp-1* mutant plants shows shorter roots and stunted growth but phenotype is weaker than *trs33-1* mutant. Scale bar = 1 cm.

G. Six-week old plants show both *tripp-1* and *trs33-1* mutants exhibit complete sterility phenotypes. Scale bar = 1 inch.

946

Figure 6. The *tripp-1* mutant exhibits photomorphogenic developmental defects.
A. Seven-day old *tripp-1* mutant seedlings grown is 16hr light / 8hr dark, show normal hypocotyl length but shorter roots. Scale = 1 cm
B. and **C.** Quantitation of hypocotyl and root lengths in seven-day light (6hr light/8hr dark) grown seedlings (n=10). Data reported as means ± SEM *P <0.05 compared to WT control (t-test).
D. Five-day old *tripp-1* mutant seedlings grown in the dark show shorter hypocotyls and longer roots than WT. Scale bar = 1cm
E. and **F.** Quantitation of hypocotyl and root lengths in 5-day dark-grown seedlings (n=10). Data reported as means ± SEM *P <0.05 compared to WT control (t-test).

956   **G**. Hypocotyl of five-day dark grown *tripp-1* mutant seedlings stained with propidium iodide show a
957   disruption in cell elongation. Scale bar 150 µm. Imaged at hypocotyl elongated zone (lower section of
958   hypocotyl).
959   **H**. Hypocotyl of seven-day light grown seedlings, stained with PI show similar cell growth between *tripp-1*
960   and WT. Scale bar 150 µm. hypocotyl-root junction at bottom section of image.
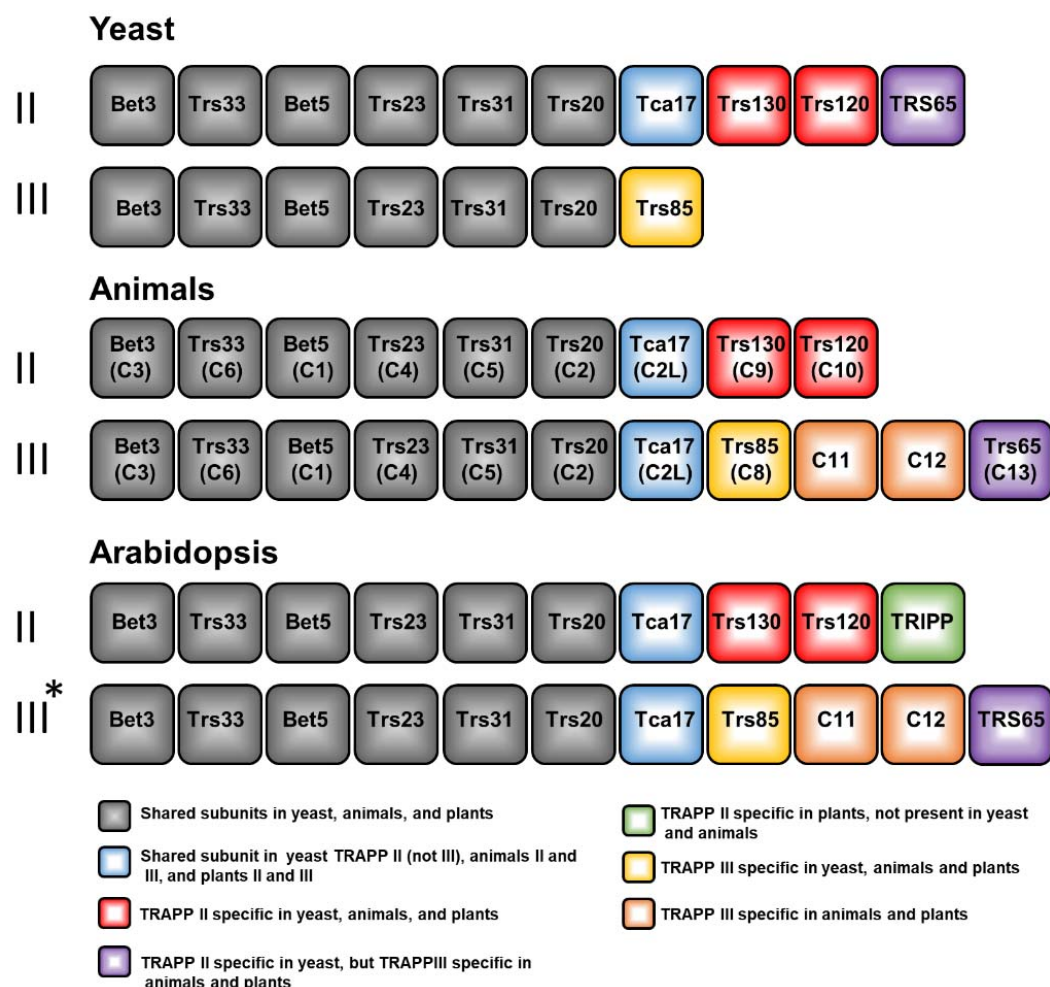961

962

963

964

965

966

967

968

969

970

Figure 7. The subunit composition of TRAPP complexes in yeast, animals and Arabidopsis.
Overview of the shared and specific subunits for TRAPPII and TRAPPIII present in different kingdoms, with the current report supporting similar TRAPP complex composition in plants. For simplicity original yeast subunit nomenclature is used and in parenthesis the names given to animal homologs for each subunit or only animal-specific names if not present in yeast. Yeast and animal TRAPPII and TRAPPIII complexes have been well defined in previous studies (Thomas et al., 2018; Riedel et al., 2018; reviewed by Kim et al., 2016; Sacher et al., 2018). TRAPP II in plants is defined from the TRIPP IP-MS results presented in this study (Table II). *TRAPPIII in plants is suggested based on the observation that AtTRS33 pulls down all TRAPP subunits (Table I) whereas TRIPP pulls down only the TRAPPII complex but not the TRAPPIII-specific-subunits (Figure 3A and supplemental TABLE II), using the animal orthologous TRAPPIII complex as reference.

982

983

984